Two-Phase Flow Modelling and Experimentation 1995
G.P. Celata and R.K. Shah (Editors)

TWO-PHASE FLOW AND BOILING, INSIGHTS AND UNDERSTANDING BY MODERN NON-INVASIVE MEASURING TECHNIQUES

F. Mayinger
Lehrstuhl A für Thermodynamik
Technische Universität München

ABSTRACT - Boiling and phase interface interactions go along with very quickly changing phenomena. Conventional measuring techniques, like thermocouples are usually to slow to get a good insight into bubble dynamics ore exchange processes between the phases and mechanical sensors disturb the effects. Therefore non-invasive and inertialess measuring techniques are needed.

Examples are presented, how optical techniques, like holographic interferometry and high-speed cinematography and also impedance probes can provide a better understanding of boiling and two-phase flow phenomena.

1. INTRODUCTION

In a channel, starting with subcooled boiling and ending with spray cooling, several zones of heat transfer mechanisms and two-phase flow patterns can be observed, like subcooled boiling, saturated boiling with various phase distributions, dry-out and post-dry-out heat transfer with spray cooling of the hot wall.

Two areas of such a channel are of special interest, because the heat transfer mechanisms and also the fluiddynamic phenomena are not yet well understood. These are the areas of subcooled boiling and of post-dry-out heat transfer. In these areas we need additional insights for being able to describe the thermohydraulic conditions in a better and more reliable way and to develop correlations on a better physical basis.

Other conditions, where we need better understanding, are highly transient flows, for example with flashing during depressurization or high velocity situations with large momentum exchange between the phases.

Usual measuring techniques for recording fluiddynamic data in two-phase mixtures, either disturb the effects to be studied, because they work on an invasive basis or they are to slow to record instantaneously the phenomena of interest. For many years, optical methods have been well known for their non-invasive and inertialess way of working, but until recently data sampling was very arduous. The enormous advances in electronic data processing today enable the engineer to handle optical informations much quicker and modern data acquisition systems make it possible to gain detailed insight into the nature of physical phenomena. So optical techniques are expected to experience an area of renaissance.

But also signals of electrical fields, for example by detecting the difference of the dielectric constant of vapour and liquid, are also frequently used in the literature. These so-called capacitive or impedance techniques can also be designed to work non-invasively.

2. SUBCOOLED BOILING

With high heat fluxes from the wall there exists a considerable temperature gradient in the boundary layer with a peak temperature at the wall, well above the saturation temperature of the liquid. This results in a nucleation and bubble formation in the superheated zone of the boundary layer. As soon as a bubble has grown to a diameter, larger than the thickness of the boundary layer, or as soon as a bubble is detaching from the wall and travelling out of the boundary layer, it starts to condense again, because it reaches the subcooled bulk. So the void fraction in this part of the boiler tube is a result of the equilibrium between bubble formation and bubble condensation.

However, there is also another phenomena, affecting local void fraction, namely the slip between the phases. Due to the velocity distribution across the pipe diameter, bubbles near the wall are adhering they, travel slower than bubbles in the bulk of the flow. This velocity profile in connection with the vapour distribution influences the void fraction, because with high velocity the same amount of fluid can be transported in a narrower area than with slow velocity. If we measure a local void frac-

tion with a capacitive method, which is described in chapter 3, along the length of the tube we get a void distribution, as demonstrated in Fig. 1 (Bräuer, Stängl, Mayinger, 1990 [1]).

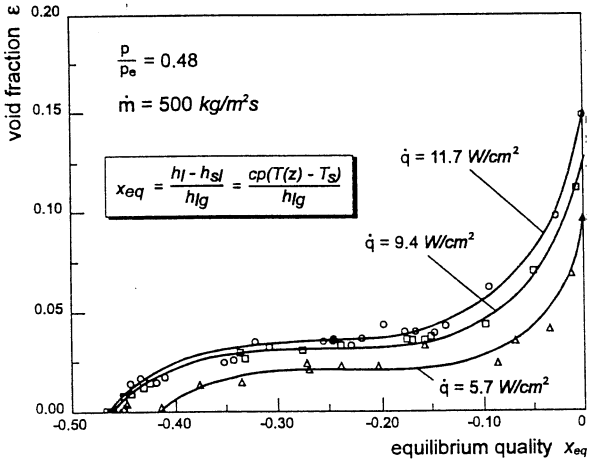

Fig. 1: Local void fraction with subcooled boiling.

In this figure, the abscissa does not represent the length and by this the travelling path of the fluid through the tube directly, but the equilibrium quality of the liquid is plotted there. The tube was uniformly heated and therefore this equilibrium quality only differs by a constant factor - depending on the heat flux and the circumference of the tube - from the length coordinate of the tube. Negative equilibrium qualities mean, that the liquid is subcooled. The measurements presented in this figure were performed with the refrigerant R12.

After very first nucleation, which starts at high subcooling in the example, shown in Fig. 1, void fraction starts to grow rapidly. After a short distance from this onset of nucleation, the gradient of the void fraction becomes much smaller until it is increasing again, when approaching saturation conditions. Reasons for these variations in the gradient of the void fraction are competitive effects between bubble growth and bubble condensation, as well as slip conditions between the phases. For better understanding of the phenomenon we have to look for the bubble dynamics at the wall.

To get a better insight into the very highly transient phenomena of bubble dynamics in subcooled boiling, we need an inertialess method, which should be non-invasive to avoid disturbing of the flow or the nucleation. Such a method is the holographic interferometry together with high speed cinematography.

2.1 High Speed Holographic Interferometry

Holographic methods are very commonly in use today and therefore only a few words should be said about the principles of this technique. Holography is an image-forming technique and can be applied for studying multi-phase fluiddynamic processes or together with interferometry to measure heat and mass transfer. In Fig. 2 the holographic two-step image-forming process of recording and reconstructing an arbitrary wave front is illustrated. The object is illuminated by a monochromatic lightsource and the reflected or scattered light falls directly onto a photographic plate. This object-wave usually has a very complicated wave-front. According to the principle of Huygens, one can, however, regard it to be the superposition of many elementary spherical waves. In order to simplify the matter, only one wave is drawn in Fig. 2.

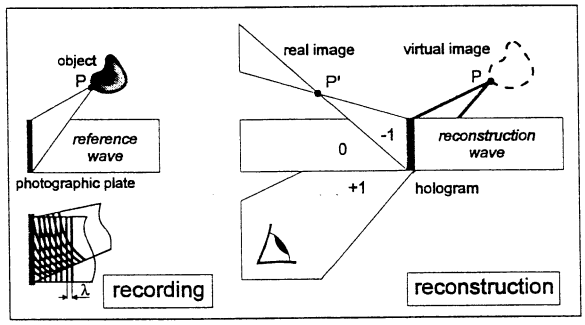

Fig. 2: Principle of holographic two-step image-forming process.

A second wave called „reference-wave" is superimposed on the first one. If the waves are mutually coherent, they form a stable interference pattern, when they meet on the photographic plate. This system of fringes can be recorded on the photographic emulsion. The amplitude is recorded in the form of different contrast of the fringes and the phase in the spatial variations of the pattern.

If the plate, after chemical processing, is illuminated by a light-beam, similar to the original reference-wave, the microscopic pattern acts like a diffraction grating with variable grating constant. The light transmitted consists of a zero-order wave, travelling in the direction of the reconstructing beam, plus two first-order waves. One of these first-order waves travels in the same direction as the original object-wave and has the same amplitude and phase distribution. This first-order wave produces a virtual image in the front of the holographic plate, seen from the side of the incoming reference beam. The other wave goes in the opposite direction and creates a real image of the object behind the photographic plate. This real image can be studied with various reconstruction devices, such as a microscope.

By using the recording capabilities of holography, different waves - even those shifted in time - can be stored in the same holographic plate. If the developed holographic plate is illuminated with the reference wave, all object waves are reconstructed simultaneously. Were they differ only slightly from each other, interference pattern are observed. These are the fundamentals of holographic interferometry.

In heat transfer, the temperature distribution in a fluid is of special interest. To investigate processes with heat transfer, a so called through light method is used, where the object wave is radiating through a volume, in which the transport process takes place. An exemplary arrangement for holographic investigations is shown in Fig. 3. A beam splitter divides the laser-beam into an object wave and into a reference wave, which is also called comparison wave. Both waves are expanded to parallel wave bundles behind the beam splitter via

lenses. The expanded and parallel organised object wave travels through the space, with the researched object of interest, called test section in Fig. 3. In this test-section, the distribution of the temperature is of interest. The reference wave bypasses the test section and falls directly onto the photographic plate.

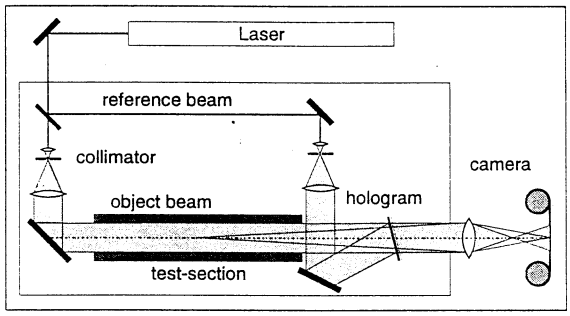

Fig. 3: Optical set-up for holographic interferometry.

There are many possibilities for arranging the optical set-ups to form a holographic interferometer, which cannot be discussed here in detail. Reference is therefore made to the literature (Mayinger 1993 [2], Mayinger and Panknin 1974 [3] and Panknin 1977 [4]).

Several procedures exist to produce interferograms. Here only one method will be explained, which can also be used in connection with high-speed cinematography. It is called the „real-time method", because it observes the process to be investigated in real time and continuously. The method is illustrated in Fig. 4.

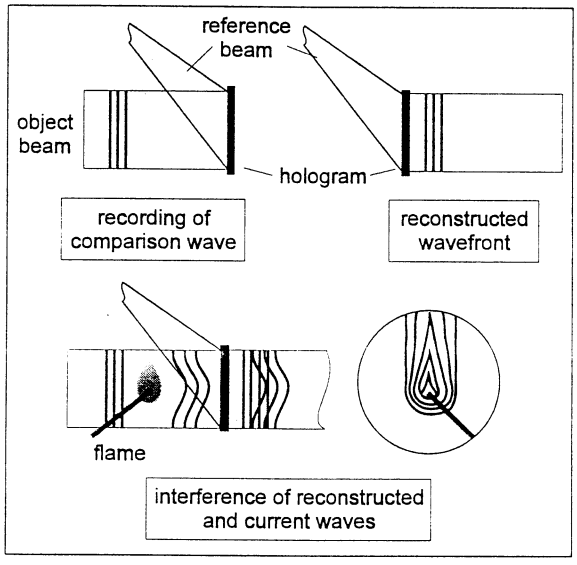

Fig. 4: Real-time method for holographic interferometry.

After the first exposure, by which the comparison wave is recorded and during which no heat transfer is going on in the test-section, the hologram is developed and fixed. Remaining at its place or repositioned accurately, the comparison wave is reconstructed continuously by illuminating the hologram with the reference wave. This reconstructed wave, showing the situation without heat transfer in the test-section, can now be superimposed onto the momentary object-wave. If the object-wave is not changed, compared to the situation before and if the hologram is precisely repositioned, no interference fringes will be seen on the hologram.

Now the heat transfer process can be started. Due to the heat transport, a temperature field is formed in the fluid and the object-wave receives an additional phase shift, when passing through this temperature field. Behind the hologram, both waves interfere with each other and the changes of the interference pattern can be continuously observed or photographed even by high-speed cinematography.

2.2 Heat Transfer at the Phase Interface of Condensing Bubbles

An example of holographic interferograms, taken with this method, is illustrated in Fig. 5. This example shows a simple flow boiling process, where subcooled water was slowly flowing over a horizontal, electrically heated surface. Due to the heating, nucleation started in the superheated boundary layer and bubbles were forming. The black and white fringes in the interferograms represent in a first approximation lines of constant temperature. The temperature difference between two black lines is constant all over the interferogram. So these interference fringes mediate an image of the temperature field. Were the fringes are closely together, a steep temperature gradient exists and if they are far apart, there is almost constant temperature in this area.

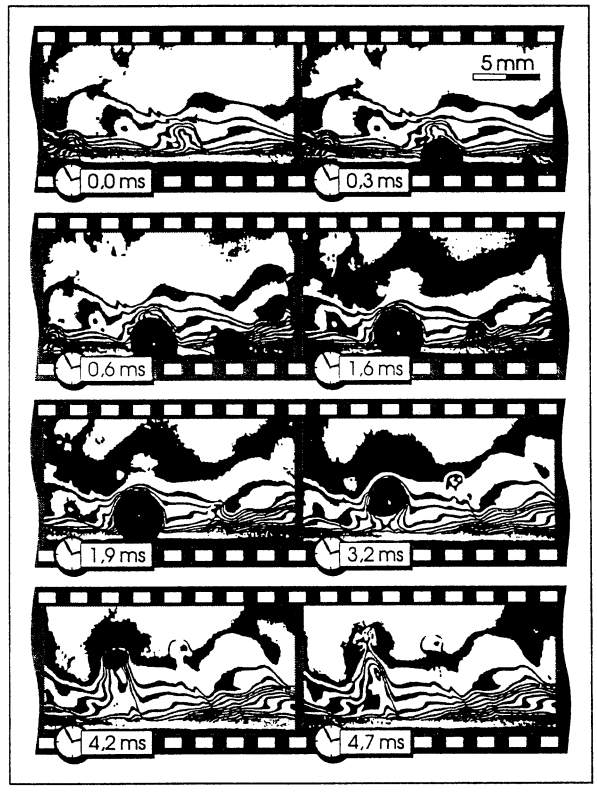

Fig. 5: Detachment and recondensation of bubbles under various boundary conditions.

Boiling on a heated surface is a statistical process and nucleation as well as recondensation of a forming bubble cannot at all be described by a simple theory. This is demonstrated in this figure also. The sequence of interferograms presented there, covers a total timespan of approximately 5 ms.

In the middle of the first interferogram, we observe a relatively thick boundary layer with flat temperature distribution. There a bubble starts to form (0,3 ms), grows and recondenses again after reaching the subcooled bulk of the fluid. Growth and recondensation of this bubble is finished after 4,7 ms.

Another bubble also at the moment of 0,3 ms starts to grow under a position of the boundary layer with high temperature gradient. Due to the high temperature gradient, this bubble grows explosively within 0,3 ms, moves very fast into the subcooled bulk and condenses there as rapidly as it was grown. Its total life span is less than a half of that of the first bubble.

So for a theoretical description of bubble growth and bubble condensation, we would need a very sophisticated information about the temporarily and locally very fast changing situations in the boundary layer. With our present mathematical tools and our limited knowledge about turbulence a reliable and precise description of the boundary layer is not possible according to my opinion. The situation becomes even more difficult, if we would like to describe the phase interface phenomena, when the bubble recondenses. But also for measuring these phenomena with holographic interferometry, we need a more optical arrangement.

With very high heat transfer coefficients, the boundary layer at a heat transferring surface becomes very thin, down to a few hundreds of a millimetre. In this case, a slightly altered method, the so called „finite-fringe-method", offers some benefits. In this method, after the reference hologram was produced, a pattern of parellel interference fringes is created by tilting the mirror in the reference wave of Fig. 6, or by moving the holographic plate within a few wave-length.

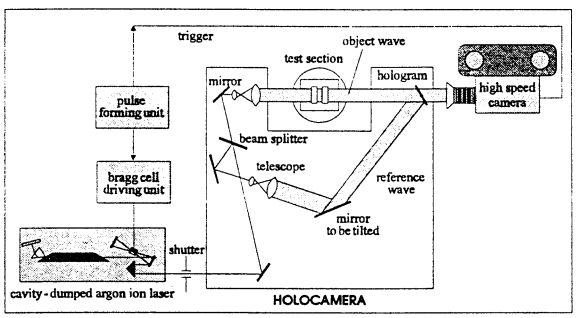

Fig. 6: Finite fringe method for holographic interferometry.

The direction of the pattern can be selected as one likes and it only depends on the direction of the movement of the mirror or of the holographic plate. By imposing a temperature field, due to a heat transport process, this pattern of the parallel interference fringes is then distorted. The distortion or deflection of each fringe from its original parallel direction is a measure for the temperature gradient at this spot and allows to deduce the heat flux and by this the heat transfer coefficient.

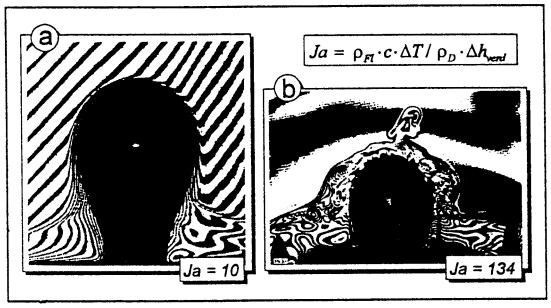

Fig. 7: Phase interface boundary layers with heat transfer- and inertia controlled condensation.

In Fig. 7, this method is applied for monitoring the boundary layer and by this also the heat transfer at the phase interface at a bubble, filled with saturated vapour and condensing in an isothermal, subcooled liquid of the same substance (Nordmann, Mayinger, 1981 [5]). The velocity of the condensation and by this the movement of the phase interface can be controlled either by the heat transfer process or, with very high subcoolings, by inertia forces. The left interferogram in Fig. 7 demonstrates the situation, when the heat transfer dominates and the right one gives an impression of inertia controlled condensation. In the latter case, the heat transfer coefficient cannot be measured by the holographic interferometry, because there is no laminar boundary layer at the phase-interface.

The interferogram on the left-hand side has to be interpreted in such a way, that in these areas, where the interference fringes have a constant gradient (parallel lines), there is a homogenous temperature field. When the temperature changes due to heat transfer, these parallel lines are deflected and the change from the original direction - the deflection of the fringe - can be used for evaluating the local and instantaneous heat transfer coefficient.

The quantitative evaluation of these finite fringe interferograms and also of the fringe pattern, shown in Fig. 5 and by this the transformation of the interference pattern into local heat transfer coefficient is a very complicated process, which cannot be explained here. Reference is made to the literature, for example: Mayinger (1994) [6], Mayinger and Panknin (1974) [3], Nordmann, Mayinger (1981) [5] and Chen, Nordmann, Mayinger (1991 [7]).

A sequence of evaluations of such interferograms is presented in Fig. 8. It was taken by combining the holographic interferometry with the high-speed cinematograhy. This combined method allows instantaneous and local measurements of the heat transfer coefficient with good accuracy.

Saturated steam was blown through a capillary into slightly subcooled water. A bubble is formed at the outlet of the capillary and the condensation process starts immediately. For a short period (No. 2 in Fig. 8) the condensation at the phase interface reduces the volume of the bubble to such a large extend, that there cannot be enough steam fed into the bubble via the flow through the capillary. Therefore, during the period „2", the

bubble takes a „squatting position", which increases the thickness of the boundary layer at the top of the bubble. This again results in a strong decreasing of the heat transfer coefficient there, because the boundary layer consists of saturated liquid. Now the steam, flowing from the capillary, can overcome the condensation rate, and the bubble is growing again. This goes together with an increasing of the heat transfer coefficient. Finally the bubble separates from the nozzle and leaves the area, where the holographic interferometry could watch the phenomena. The heat transfer coefficient at the side of the bubble is much smaller than at its top, as Fig. 8 also shows.

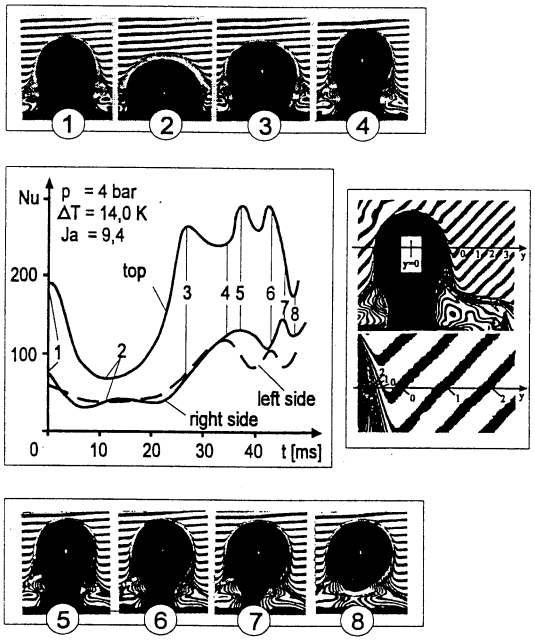

Fig. 8: Heat transfer at the phase interface of a vapour bubble, condensing in a subcooled liquid, deduced from a sequence of interferograms.

The reason is, that the boundary layer, starting to be formed at the top, becomes thicker via the equator, when the bubble is growing and moving upwards into the subcooled bulk.
It looks very complicated to describe the local and temporal variations of the heat transfer coefficient with a correlation. However, the situation becomes much simpler if one is only interested in the average heat transfer coefficient - averaged versus time and circumference of the bubble. Data for the average heat transfer coefficient with condensing bubbles are shown in Fig. 9, where the Nusselt-number is plotted versus a dimensionless subcooling, expressed in the terms of the Jakob-number.

$$Ja = \frac{\rho_L \cdot c_L \Delta T_{sub}}{\rho_V \Delta h_{LV}}$$

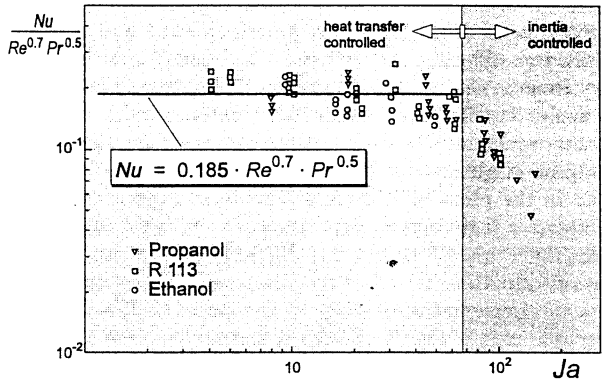

Fig. 9: Heat transfer at the phase interface of a condensing bubble.

As Fig. 9 demonstrates, the heat transfer coefficient can be satisfactorily described by a simple equation, using the Reynolds- and the Prandtl-number as variables, as long as heat transfer controls the condensation. At high Jakob-numbers - above 70 - inertia-controlled phenomena start to dominate and then of course the measuring method and also the equation fail.

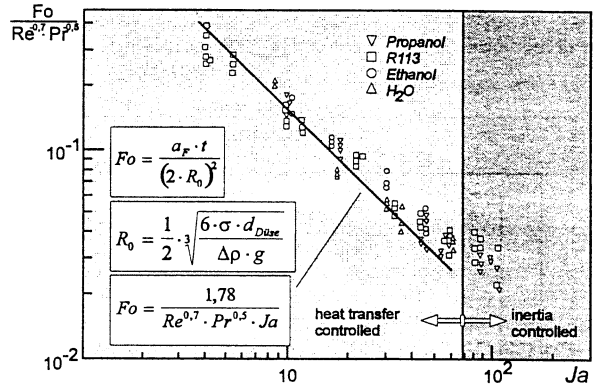

Fig. 10: Dimensionless condensation time of a bubble.

In a similar simple way, the life span of a condensing bubble, formed out of a capillary by vapour flow, can be described, as Fig. 10 shows, where the dimensionless lifetime, in form of the Fourier-number, is plotted versus the Jakob-number (Chen 1985 [8]).

3. POST DRY-OUT HEAT TRANSFER

Dispersed flow film boiling is of great importance in many industrial applications, for example in the design and operation of once-through steam generators in the analysis of a hypothetical loss-of-coolant accident in nuclear reactor systems and in the evaluation of some metallurgical and cryogenic processes. The heat transfer mechanism of dispersed flow in the high wall-superheat-region has been well investigated for simple geometry, mostly for stright tubes.

The situation changes if the dispersed flow travels through a bend. In addition to momentum and gravity-forces, centrifugal forces are acting on the liquid phase. Even in a simple circular bend - a common flow geometry in practise - the mechanism of dispersed flow heat transfer is still fully understood. Centrifugal forces may create secondary flow also and dispersed flow dynamics may be subjected to changes in the bulk flow structure and in the phase distribution. To understand these phenomena a little better, experiments were carried out by Mayinger and Wang (1994) [9] in a refrigerant (R12) two-phase flow test facility. Dispersed flow was produced through the dry-out of the annular flow in the vertical part of the joule-heated test section. The dry-out point was regulated to occur at a position 2,5 m before the bend inlet to allow a sufficient length of dispersed flow development. So the test section consists of a vertical part and a 90° bend. The tube and the bend were made of stainless steel, having an inner diameter of 28,5 mm and a wall thickness of 2,6 mm.

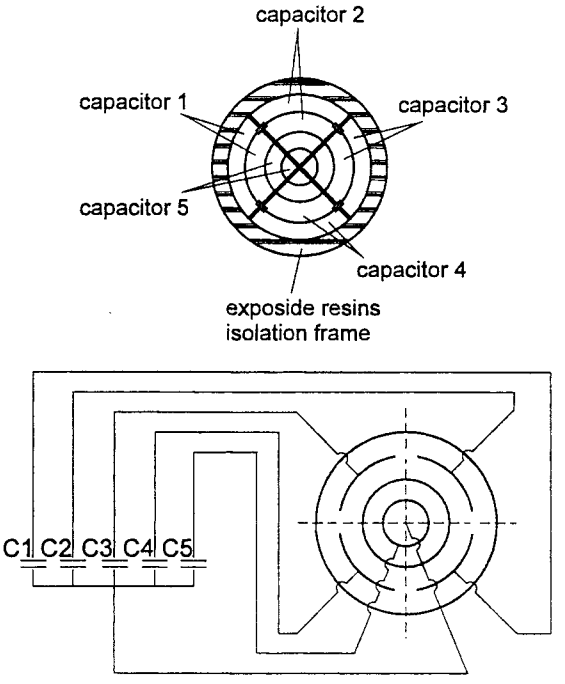

Fig. 11: Structure of the impedance probe

An impedance probe was used to measure the local liquid fraction in 5 different regions of the cross section. Fig. 11 shows the structure of the probe. It was composed of 4 thin concentric rings, divided and wired together to constitute 5 separate capacitors, in which a nearly homogeneous electric field could be established. Different capacitors were electrically isolated and supported by an epoxide frame. Supplied with 1 MHz high frequency voltage, the dielectric field between these capacitors was measured by a high precision capacitance meter. According to Maxwell's theoretical analysis on dispersed droplet flow, the liquid fraction 1-ε can be deduced from the two-phase dielectric constant via capacitance measurements. Wang (1993) [10] provided an error analysis of this measuring technique. He revealed, that the impedance probe gives a good indication of liquid fraction, even if there is a thin liquid film forming on one of the electrodes due to droplet impingement. The design of the impedance probe, shown in Fig. 11 is mechanically slightly interacting with the flow. A better, non-invasive design will be presented in chapter 4. In the experiments a remarkable change of the bulk flow structure and of the droplet dynamics was observed due to the centrifugal forces and also due to the secondary flow, produced by the bend.

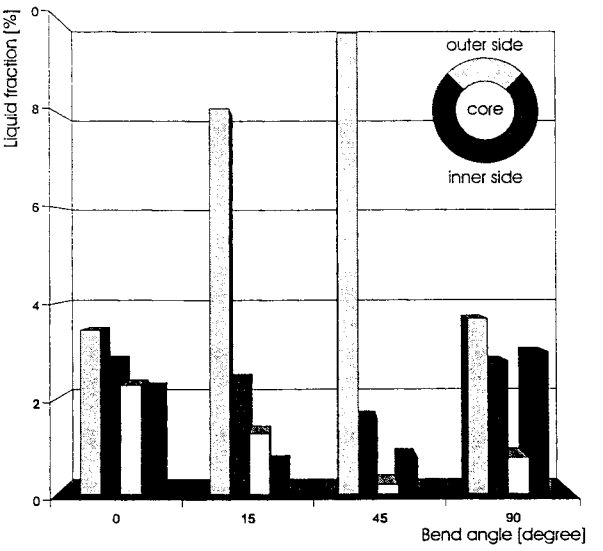

Fig. 12: Phase distribution in a bend with dispersed flow.

Fig. 12 shows the change in the phase distribution along the path of the flow through the bend for a total mass flow rate of 1240 kg/m^2. The experiments showed, that phase separation, due to the centrifugal effect, appears immediately after the bend inlet. The liquid fraction increases significantly from 0° to 15° in the outer side region, whereas it decreases correspondingly in the inner side region. Dispersing continues until 45° bend angle, where the effect of the secondary flow reversal becomes noticeable. Fig. 12 shows, that a large amount of liquid appears in the inner region, near the bend outlet. This fact of liquid redistribution can be explained by a liquid film invert reversal along the wall.

Centrifugal forces - like gravity forces - produce a pressure force, acting in a opposite direction. The droplets in the bulk of the flow are mainly affected by the centrifugal force and they therefore are moving outwards. On the other side, particles in the boundary layer near the wall, where friction has a high influence, may follow the pressure force and by this they are slowly moving inwards.

This change in the phase distribution can have a significant influence on the heat transfer coefficient along the wall in the bend. Especially under intermediate and large mass fluxes, together with low heat fluxes, this migration of the droplets and also of the liquid particles in the boundary layer near the wall may result in a re-wetting of the wall. Due to a massive droplet impingement, the outer wall may be quickly quenched to a value

near the saturation temperature resulting in an order-of-magnitude increase of the heat transfer coefficient, as can be seen from Fig. 13. Such a dramatic increase of heat transfer indicates a departure of the heat transfer mechanism from film boiling to wetting evaporation. Under low wall superheat, droplets maintain stable contact on the outer wall, where they can easily link together to form a continuous liquid film. This has been confirmed from liquid fraction measurements, shown in Fig. 12. Therefore liquid film evaporation is responsible for the heat transfer augmentation. Further downstream, because of the action of the secondary flow and the gravity, rewetting is propagated from the outer side to the inner side, where small wall superheat and high liquid fraction are observed. Also there the local heat transfer coefficient is consequently greatly enhanced.

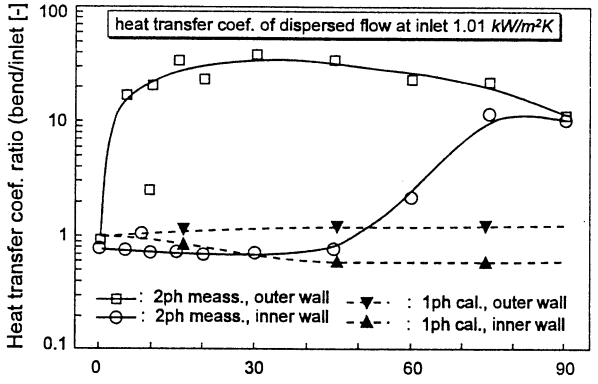

Fig. 13: Heat transfer with spray flow under rewetting status in a bend.

In Fig. 13, data are presented also, which were calculated, assuming single phase vapour flow at the wall. For information, how this calculation was performed and also about details of the measuring technique, reference is made to Wang (1993) [10].

4. HIGHLY TRANSIENT FLOW

Highly transient flow can be investigated by optical techniques, like high-speed cinematography or double pulse holography and by impedance method also.

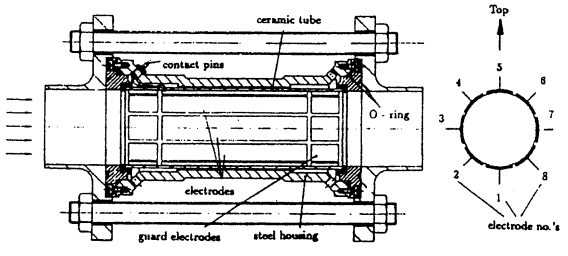

Fig. 14: Impedance sensor for void measurements.

The principles of the impedance method was briefly described in Chapter 3, however, the technique presented there has the disadvantage, that it is not working on a fully non-invasive basis. To overcome these insufficiencies a new approach was made for measuring void fraction in multi-phase flows (Klug, Mayinger, 1994 [11], 1992) [12]. This non-intrusive impedance probe consists of eight surface-plate electrodes, implemented into the inner side of a tube, as shown in Fig. 14. With this probe, the impedance between different combinations of electrodes, the so-called measuring fields, is measured, as demonstrated in Fig. 15.

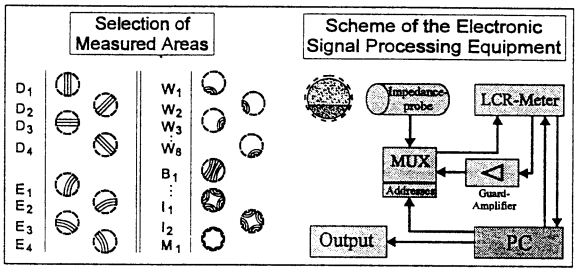

Fig. 15: Examples of measuring fields.

For every measuring field the impedance - as an integral parameter - is determined by the distribution of phases within the whole sensing volume of the probe. However, the individual domains of the sensing volume make different contributions to the total amount of the flow-influenced probe impedance. Therefore characteristic contribution patterns for the spatial sensitivity (Bair, Oakley, 1992 [13]) can be observed, which allow to classify the multitude of measuring fields into several groups.

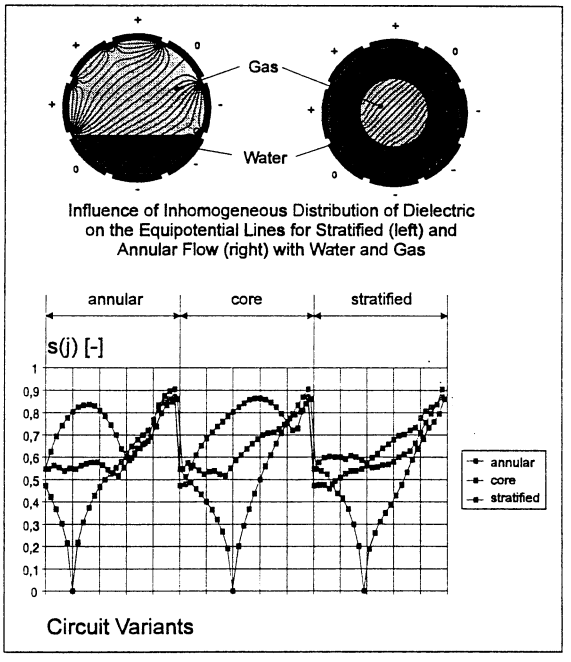

Fig. 16: Calculated derivations for 3 cases, by using 27 measuring fields.

Each group consists of a certain number of fields, which depend on the degree of field symmetry. One can distinguish between diametrical fields (D), excentric fields (E), wall fields (W), large fields (B), integral fields (I) and

Maltese cross-shaped fields (M). For each field and each flow pattern one can make a theoretical calculation and one can compare the theoretical prediction with the measured one. This comparison is a kind of calibration.

For practical use, where the flow pattern and also the void fraction are unknown, one can switch through all these mentioned field types and by comparing the measured signals with the calibration data, one finds a minimum of deviation for a certain field group and a certain flow pattern between actual measured data and calibration values. From that one knows, which flow pattern exists during the actual measurement and one can choose the right correlation for evaluating the impedance signals to get the local volumetric void fraction.

This briefly described procedure is sketched in Fig. 16 for 3 different flow patterns, namely stratified flow, annular flow and inversed annular flow (vapour outside and liquid in the bulk). The switching of the fields is done by a computer.

For bubble flow, churn flow and also fog flow, 2 or maximum 4 electrodes, integrated into the tube wall, are sufficient to get a correct reading of the void fraction. So this impedance method can be used for highly transient flow. An example of measuring void fraction in a highly transient flow is shown in Fig 17. 2 impedance probes were installed in a 1,1 m long pipe, through which a non-steady two-phase flow mixture was flowing during a blow-down process. A pressure vessel, filled partially with propane, was suddenly depressurized, feeding a liquid-vapour-mixture - due to flashing - into the pipe and flowing via an orifice into a low pressure chamber. The pipe had a diameter of 10 mm and the flow area at its down stream end was reduced by an orifice of 5 mm.

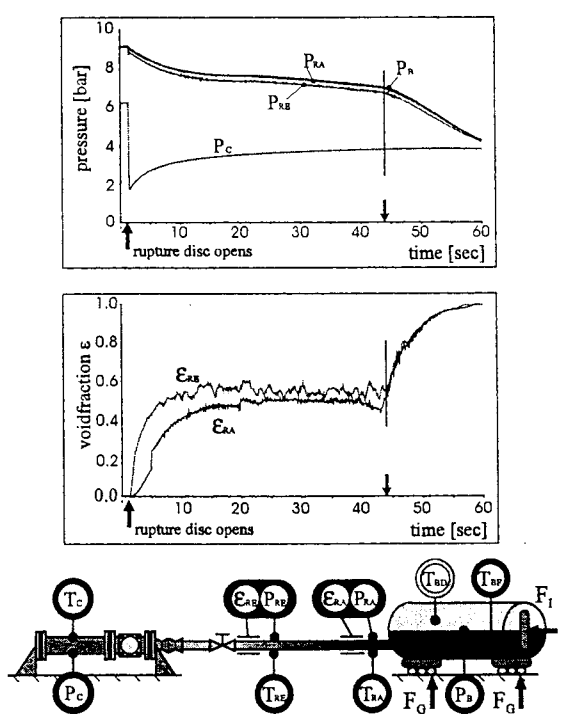

Fig. 17: Pressure and void fraction history during blow-down.

The upper part of Fig. 17 shows the temporal course of the pressure at 2 positions along the pipe, namely at the entrance, where the two-phase mixture from the pressure vessel comes in and at the downstream end, just before the orifice. The lower curve in the upper diagram of Fig. 17 presents the pressure in the low pressure chamber, which is slightly increasing due accumulation of the two-phase mixture.

The lower part of Fig. 17 presents quantitative data of the local void fraction at the entrance and at the exit of the pipe. At the entrance of the pipe, density wave oscillations can be observed for a period of almost 20 s, approximately 10 s after the blow-down started. These density wave oscillations are resulting from a fluiddynamic disequilibrium between the mass flow rate, approaching the pipe from the pressure vessel and that, leaving it at the orifice. There is an interaction between the two-phase friction in the pipe and in the orifice on one side and the pressure difference between the pressure vessel and the low pressure chamber on the other side. High pressure difference produces violent flashing, which has high friction as consequence. Evidently these density wave oscillations are sensitive to very small pressure changes, because the pressure at the exit of the pipe - where the large density oscillations were observed - shows very little fluctuations only. Also at the entrance of the pipe, the density wave oscillations are very small. After 28 or 29 s, vapour enters the pipe from the pressure vessel and therefore the void fraction increases suddenly.

These density wave oscillations were observed at medium void fractions only - 40 to 60% - whereas at high void fractions, the two-phase mixture smoothly travels through the pipe.

If the flow is optically accessible, one can use high-speed cinematography or double pulse holography to measure size, shape and velocity of the dispersed phase by particle imaging. For details, how to handle these techniques, reference is made to the literature (Mayinger 1994 [4], Chavez 1991 [14], Chavez and Mayinger 1992 [15], Neumann and Mayinger, 1978 [16]). Here only an example shall be presented, to show how particle image velocimetry and ultra-short time imaging can give insights for improving the design of an apparatus, working with highly transient flow. To clean gas from very small particles - aerosols - gas is blown at high velocities through a venturi scrubber, which is sketched in the left lower part of Fig. 18. In the so-called throat of the venturi scrubber, i.e. in the part, where the highest gas velocity exists, washing liquid - usually water - is added to the gas flow. The usual assumption in the literature is, that this liquid is dispersed into a cloud of very small droplets by the shear stress of the gas flow, resulting in an adsorption of the aerosols by the liquid. High speed particle imaging demonstrated, that the liquid is not dispersed in droplets at the very first moment - for less than 1 ms - but the water jet disintegrates into filaments, sometimes having the form of parachutes. The upper part of Fig. 18 shows examples of such parachutes. On the left side, one and the same parachute is photographed twice within 10^{-5} s. From this double exposure, one can calculate the velocity, which in this case came out in the order of approximately 60 m/s. From this double exposure picture, one can also learn, that not al

parts of the parachute travel with the same velocity, but the membrane is flowing faster than the droplets at its upper end. This results in an overstressing of the membrane, which finally ruptures and is dispersed in many tiny liquid particles, shown on the right upper side of Fig. 18.

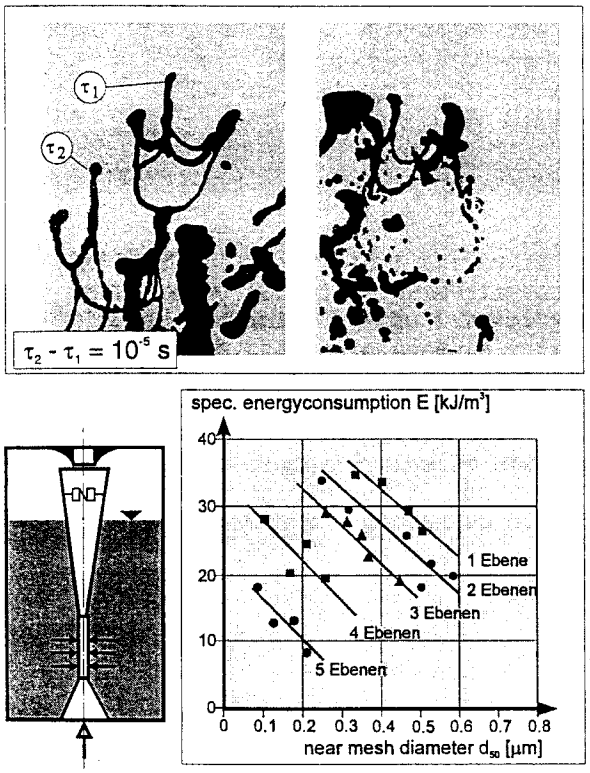

Fig. 18: Gas cleaning in venturi-scrubbers, flow conditions and separation efficiency.

This observation gives the hint, that it is advantageous to add the same amount of washing liquid, not in one level of the venturi nozzle, but to stagger it over the flow path of the gas. Doing this has two benefits. It improves the cleaning efficiency of the venturi nozzle and lowers the energy demand to operate it. This is clearly demonstrated in the lower right part of Fig. 18. Adding washing liquid in one level only, aerosols can be washed out, not smaller than 0,4 µm. Adding the same amount of liquid to the gas flow of the same velocity in 5 levels lowers the minimum aerosol size to 0,1 µm with much smaller operating energy.

CONCLUDING REMARKS

After the stone-, the brass- and the iron-age, we are no living in the silicon age and powerful computers enable us to describe two-phase flow in detail and to model phase interface phenomena. Doing this we cannot rely on intuition and imagination only. Furthermore we have to „see" what happens. Novel optical methods, but also other non-intrusive measuring techniques help us to get the needed physical insights. A former draw-back of optical measuring techniques, namely the laborious and time-consuming evaluation does not exist any more. Even a personal computer is good enough for evaluating a hologram or an interferogram within a few seconds, a process, that took several hours in the past. So a new symbiosis could come into being between theorists and experimentalists, working in boiling and in multi-phase flow.

REFERENCES

1. Bräuer, H., Stängl, G., Mayinger, F., Onset of nucleate boiling with R12, Proc. of the 9th Int. Heat Transfer Conf., Hemisphere Publ. Corporation, Vol. 3, 1990, S. 419-424.
2. Mayinger, F., Image-forming, optical Techniques in Heat Transfer: Revival by computer-aided Data Processing, Journal of Heat Transfer, Trans. of the ASME, Vol. 115, 1993, pp. 824-834.
3. Mayinger, F., Panknin, W., Holography in Heat and Mass Transfer, Proceedings of the Fifth International Heat Transfer Conference, 1974, Vol. VI, pp. 28-43.
4. Panknin, W., Eine holographische Zweiwellenlängen-Interferometrie zur Messung überlagerter Temperatur- und Kondensationsgrenzschichten, Ph.D. Thesis, 1977, Technische Universität Hannover, Germany.
5. Nordmann, D. and Mayinger, F., Temperatur, Druck und Wärmetransport in der Umgebung kondensierender Blasen, VDI-Forschungsheft 605, 1981.
6. Mayinger, F., Optical Measurements, Techniques and Application, Springer Verlag, Heidelberg, (1994).
7. Chen, Y.M., Nordmann, D., Mayinger, F., Heat Transfer at the phase interface of condensing bubbles, In: Phase interface phenomena in multiphase flow. Eds.: Hewitt, G.F., et. at. New York, Hemisphere, 1991, pp. 433-442.
8. Chen, Y.M., Wärmeübergang an der Phasengrenze kondensierender Blasen, Ph. D. Thesis, 1985, Technische Universität München, Germany.
9. Mayinger, F., Wang, M.J., On the Mechanism of Dispersed Flow Heat Transfer in the circular Bend., Proceedings of the 10th Intern. Heat Transfer Conference, Brighton 1994, Vol. FB 17, pp. 503-508.
10. Wang, M.Y., Phasenverteilung, Sekundärströmung und Wärmeübergang bei Sprühkühlung in Krümmern, Ph. D. Thesis, 1993, Technische Universität München, Germany.
11. Klug, F., Mayinger, F., Impedance based flow reconstruction - A novel flow composition measuring technique for multi-phase-flows, Nuclear Engineering and Design, 146, pp. 35-42 (1994).
12. Klug, F. and Mayinger, F., Proc. NURETH-5 Meeting, Salt Lake City, Sept. 21-24, 1992 (1992).
13. Bair, M.S. and Oakley, J.P., 1st Meeting European Concerted Action on Process Tomography, Manchester 26-29th, 1992 (1992).
14. Chávez, A., Holographische Untersuchung an Einspritzstrahlen - Fluiddynamik und Wärmeübergang durch Kondensation, Diss. Techn. Univ. München 1991.

15. **Chávez, A., Mayinger, F., (1992), Measurement of direct-contact condensation of pure saturated vapour on an injection spray by applying pulsed laser holography, Int. J. Heat Mass Transfer, Vol. 35, No. 3, pp. 691-702, 1992.**
16. **Neumann, M., Mayinger, F., Staubabscheidung in Venturi-Wäschern, German Chemical Engineering, Vol. 1, Nr. 5, 1978, S. 289-293.**